BBA - Bioenergetics 1862 (2021) 148446

Contents lists available at ScienceDirect

BBA - Bioenergetics

journal homepage: www.elsevier.com/locate/bbabio

Proton exit pathways surrounding the oxygen evolving complex of photosystem II

Divya Kaur [a,b], Yingying Zhang [b,d], Krystle M. Reiss [c], Manoj Mandal [b], Gary W. Brudvig [c], Victor S. Batista [c], M.R. Gunner [a,b,d,*]

[a] Department of Chemistry, The Graduate Center, City University of New York, New York, NY 10016, United States
[b] Department of Physics, City College of New York, NY 10031, United States
[c] Department of Chemistry, Yale University, New Haven, CT 06520, United States
[d] Department of Physics, The Graduate Center of the City University of New York, New York, NY 10016, United States

ARTICLE INFO

Keywords:
Proton transfer
Photosystem II
Oxygen evolving complex (OEC)
Hydrogen bond network.
Water channels
MCCE

ABSTRACT

Photosystem II allows water to be the primary electron source for the photosynthetic electron transfer chain. Water is oxidized to dioxygen at the Oxygen Evolving Complex (OEC), a Mn_4CaO_5 inorganic core embedded on the lumenal side of PSII. Water-filled channels surrounding the OEC must bring in substrate water molecules, remove the product protons to the lumen, and may transport the product oxygen. Three water-filled channels, denoted large, narrow, and broad, extend from the OEC towards the aqueous surface more than 15 Å away. However, the role of each pathway in the transport in and out of the OEC is yet to be established. Here, we combine Molecular Dynamics (MD), Multi Conformation Continuum Electrostatics (MCCE) and Network Analysis to compare and contrast the three potential proton transfer paths. Hydrogen bond network analysis shows that near the OEC the waters are highly interconnected with similar free energy for hydronium at all locations. The paths diverge as they move towards the lumen. The water chain in the broad channel is better connected than in the narrow and large channels, where disruptions in the network are observed approximately 10 Å from the OEC. In addition, the barrier for hydronium translocation is lower in the broad channel. Thus, a proton released from any location on the OEC can access all paths, but the likely exit to the lumen passes through PsbO via the broad channel.

1. Introduction

Photosynthetic organisms use solar energy to reduce atmospheric CO_2 to sugar, generating oxygen as a byproduct. Water is the ultimate source of reducing of equivalents (i.e., electrons). The difficult water oxidation reaction is catalyzed by the oxygen evolving complex (OEC) of photosystem II (PSII), an inorganic Mn_4CaO_5 cluster ligated by the side chains of surrounding amino acid residues (Fig. 1C) [1–4]. The OEC cycles through five increasingly oxidized states, S_0, S_1, S_2, S_3 and S_4 to permit O—O bond formation in the transition from S_4 to S_0 [1–3,5,6]. The overall reaction is:

$$2H_2O + 2PQ + 4H^+_{stroma} + 4h\nu \rightarrow O_2 + 2PQH_2 + 4H^+_{lumen}$$

resulting in the release of four protons to the lumen while the protons needed for reduction of the two equivalents of plastoquinone (PQ) to plastoquinol (PQH_2) are taken up from the stroma. Thus, the reaction generates a carrier of reducing equivalents (PQH_2) and a transmembrane pH gradient used to fuel ATP synthesis and other processes [7]. PQH_2 then reduces the cytochrome b_6f complex, which in turn passes electrons to flavodoxin via PSI and then to $NADP^+$ at the end of the light activated photosynthetic electron transfer chain.

The OEC is embedded in the PSII D1 subunit about 20 Å from the lumen, the outer, positive side of the chloroplast membrane. Thus, substrate water molecules must be delivered to the OEC and the product protons and O_2, must be removed. However, the route for these transfers remains to be established. The crystal structures show long, complex water filled through the protein, hydrogen bond networks that might serve for the required functionality [4], including three channels commonly known as narrow, broad and large channels (Fig. 1A and B) [8–12].

Water diffusion from the lumen to the OEC almost certainly is via water-filled channels. Diffusion of O_2 away from the OEC could happen

* Corresponding author at: Department of Physics, City College of New York, 160 Convent Avenue, New York, NY 10031, United States.
E-mail address: mgunner@ccny.cuny.edu (M.R. Gunner).

https://doi.org/10.1016/j.bbabio.2021.148446
Received 28 January 2021; Received in revised form 29 April 2021; Accepted 1 May 2021
Available online 5 May 2021
0005-2728/

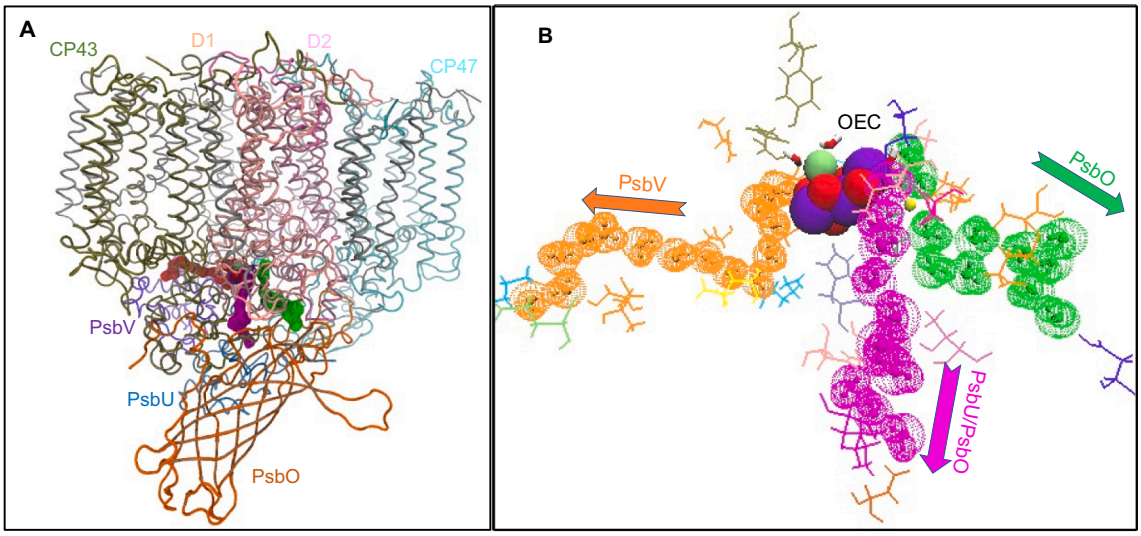

Fig. 1. Structure of PSII and water channels. (A) Monomeric PSII highlighting D1, D2, CP43, CP47 and PsbO subunits (4UB6). The OEC cluster and water channels are shown as spheres. The entire PSII monomer embedded in a lipid bilayer is included in the MD trajectory. (B) Water molecules in the large (orange), narrow (magenta) and broad (green) channels taken from one snapshot in the MD trajectory.

even through relatively hydrophobic paths [13,14], while protons typically diffuse through chains of waters and selected polar amino acids via the Grotthuss mechanism [15].

Grotthuss competent waters and side chains can serve both as hydrogen bond donors and acceptors to transfer a proton rapidly through highly-organized hydrogen bond networks [16]. A group in the middle of a Grotthuss proton transfer chain will be a hydrogen bond acceptor to a group towards the proton source and a donor to a group nearer the exit. Proton transfer shifts the proton to the adjacent hydrogen bond acceptor (nearer the exit) and accepts the proton from its hydrogen bond donating neighbor (nearer the proton input site). An excess proton can thus move rapidly through a pre-aligned chain without a proton ever being trapped along the pathway. Water and the Grotthuss-competent sidechains, serine, threonine and tyrosine and neutral His, have a lone pair of electrons to accept a proton and a polar proton to pass onward [17].

Ionized Asp or Glu residues have no dissociable proton, while an ionized His, Lys or Arg have no lone pair to accept a proton so cannot participate in a Grotthuss proton transfer chain. These charged groups stabilize water molecules within internal channels and help to orient the hydrogen bond chains [18]. They can also facilitate proton transfer pathways by providing a transient proton loading site to hold and release a proton along proton transfer chains [7]. Asn, Gln and Trp can make hydrogen bonds and anchor and orient the hydrogen bonded chain but are unlikely to serve as active intermediates in proton transport.

1.1. Source of the protons released from the OEC

In the oxidation of two waters to oxygen, the OEC is oxidized four times, through five S-states and four protons are lost to the lumen. The PSII XFEL structures provide insights into how the OEC structure changes through the S-state cycle [6,19]. DFT-based QM/MM simulations have optimized the structure, hinting at the sites of proton binding within the cluster through the reaction cycle [20]. The source of the lost proton will be different in each S-state transition. Going from S_0 to S_1, the donor is likely to be an oxygen bridging two Mn, releasing a proton retained within the OEC following water oxidation in the S_4-state of the previous cycle. Thus, its location may provide information about the position of the substrate waters bound to the OEC prior to O_2 release [1,20,21]. EPR [22] and associated computational studies [23–25] favor a protonated O5 bridge (see Fig. 1B, SI S1). However, other studies have supported a protonated O4 [26–28] or O1 [29]. In all other S-states, which are more oxidized than S_0, none of the Mn-bridging oxygens retain a proton. There is little or no proton release to the lumen when S_1 is oxidized [30–32]. In the oxidation states beyond S_2, protons have been proposed to be released from the terminal waters of Mn4 (W1, W2) [33,34] or of Ca (W3, W4) [35–38] or from waters, such as W_X bound nearby [33]. The resulting hydroxyl may be inserted into the cluster as a substrate for O_2 formation [3,25,36,39–41].

The question remains what role each of the three water filled channels near the OEC plays in the transport of the substrate and products [3,9,12,42] and each has been considered as a proton exit pathway. The broad channel nominally originates from the O5 bridge in the vicinity of Mn4 and moves to the lumen via the peripheral PsbO subunit (Fig. 1). Continuum electrostatic simulations [10] showed a monotonic increase in proton affinity of acidic and basic residues moving along the broad channel to the lumen, suggesting this channel could provide a downhill path for proton exit. MD studies [42–44] of the broad channel exit identified acidic residues on the PsbO surface that can trap protons stabilizing proton release. Recent, eigenvector centrality analysis using a MD trajectory [45] of a 25-Å sphere centered at the OEC in the S_1 and S_2 states found that the narrow and broad channels are favorable for water and proton transport while the large channel may be better suited for transfer of larger ions.

The narrow channel has been assigned an origin near the OEC O4 bridge and includes the terminal water ligand, W1, of Mn4. It travels to the lumen alongside the broad channel through the interface of the PsbU and PsbO subunits (Fig. 1A and B). Several computational studies of the S_0 to S_1 transition [9,26] favored release of a proton from O4. The oriented waters entering the narrow channel make it look well-prepared to transfer protons via a Grotthuss mechanism [26,45]. However, small, neutral, polar molecules such as ammonia [46–51] and methanol [52,53] bind in this channel, suggesting that it could be the path for neutral, polar substrate water delivery. Steered MD studies [11] showed the narrow channel has the lowest barrier to water permeation. If W1 is a substrate water, it would then be well positioned to be replenished via this channel.

The large channel originates from O1, reaching the lumen in the PsbV subunit (Fig. 1A and B) [11]. It contains more hydrophobic residues than the other two, so has been proposed as the path for oxygen release [11]. MD studies [9,11] show that this channel has the highest barrier for water permeation. However, O_2 need not transfer through a water-filled channel and solvent accessible cavity analysis [9] and noble gas derivatization [8] proposed a 'back channel' as a separate, more

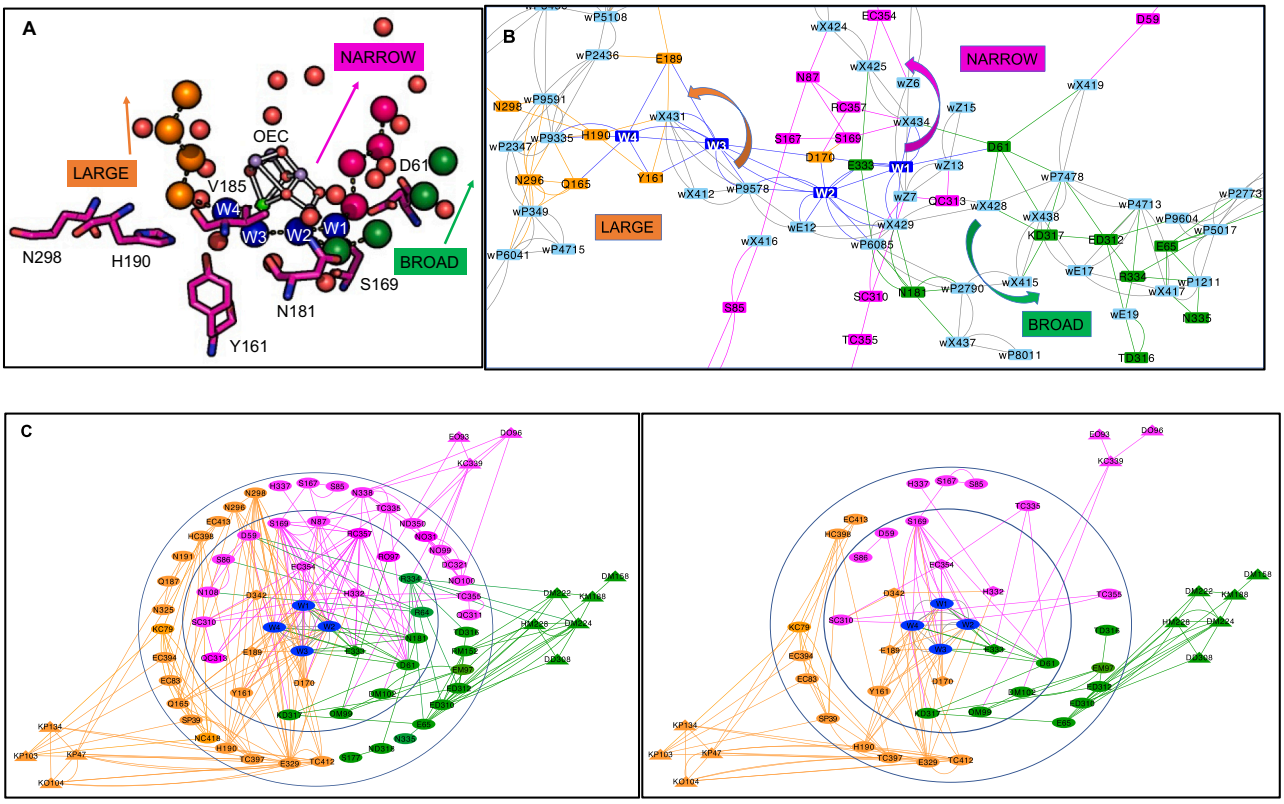

Fig. 2. Three views of the hydrogen bond network surrounding the OEC. The same colors are used in all figures. Orange: large channel; green: broad channel; magenta: narrow channel. Dark Blue: Primary water ligands to Mn4 (W1, W2) and to Ca (W3 and W4). (A) Water oxygen atoms and hydrogen bonded residues within 7 Å of the OEC. The arrows indicate the direction of each channel. Water oxygens are colored by the nearest channel. Red spheres are waters that are not clearly assigned to a channel. Table 1 give the assignment of each residue to a channel.
(B) The highly interconnected region near the OEC from the MCCE/network analysis for one representative MD snapshot. Water molecules are light blue and are labeled w, a letter and number. Water molecules with letter X, E and Z are taken from the crystal structure while those labeled P are added during MD set up so have an arbitrary number. Hydrogen bond connections made in $> 0.1\%$ of the MC accepted states are shown by connecting lines. Arrows show the direction of proton transfer towards the three separated channels. Table 2 traces several possible paths though the network to the lumen from each of the four OEC terminal waters.
(C) Network of hydrogen bond connections from the OEC to the lumen found in MCCE calculations starting from a representative MD snapshot. Nodes are labeled as: Residue type, Chain designation, Residue number. No chain designation indicates D1. Chain C is CP43; D is D2; M is PsbO; O is PsbU; and P is PsbV. For example, EC354 is CP43-Glu354. Diamonds are primary ligands and triangles are residues with at least 20% of their surface exposed to the lumen. Lines show hydrogen bond connections mediated by four or fewer waters. The inner circle encloses highly interconnected residues near the OEC. Connections between residues nominally in different channels are seen. The outer circle encloses residues in their separated channels. Beyond the outer circle are residues exiting the channel at the surface. *Left*: Nodes that contain all residues in Table 1. *Right*: Nodes that show only residues that can participate in Grotthuss proton transport or serve as proton loading sites, labeled PT in Table 2. §Fig. SI S2 provides network figures for nine additional snapshots for comparison.

hydrophobic pathway for O_2 release. Experimental [21] and computational studies [11,39] have also favored the large channel for substrate water delivery. The large channel appears to be the closest point of entry if the terminal water ligands of Ca serve as a substrate [21,39,54,55]. This channel has also been proposed to play a role in proton transfer [42,56].

Thus, the current view of the region around the OEC sees three distinct channels, each of which has been proposed to play a role in water delivery and proton release. It may also be that channels can be bifunctional or substrates and products could use multiple paths between the OEC and lumen [10,26,33]. Thus, while, several experimental and computational studies have assigned different roles of water channels i.e. the broad channel to be the proton exit channel [10,42], the narrow channel carries water [11] and the large channel carries oxygen [11], the question is by no means settled.

Here we use computational simulations to compare the ability of the three water-filled channels to transport a proton in protein structures optimized in the S_1-state [24,57]. The connection between the three channels near the OEC and the barrier to hydronium transfer through the channels are studied by combined Molecular Dynamics (MD), Multi Conformation Continuum Electrostatics (MCCE) [58] and Network Analysis [59]. The main conclusions are that all three water channels are highly interconnected near the OEC. In addition, the energy to place a hydronium in any putative water channel is also very similar near the OEC. However, moving out towards the lumen, the broad channel is energetically more hospitable for a hydronium than the large and narrow channels. Thus, a proton can exit from any point on the OEC to leave the protein via the broad channel. Likewise, the interconnections of the water channels near the OEC suggest substrate waters can enter via any channel to provide the substrate to any point on the OEC.

2. Methods

2.1. MD trajectory yields an ensemble of PSII snapshots

A monomer of PSII from the high resolution 1.9 Å crystal structure of *Thermosynechococcus vulcanus* 4UB6 is the input for MD [4]. The detailed description of the MD setup is found in SI S4. The OEC bond lengths, angles and dihedrals are taken from the QM based optimized S_1 structure [57]. The system is prepared using the CHARMM-GUI [60], which adds a water box and lipids to the protein structure while retaining the crystal water molecules. The Asp, Glu, Arg, Lys and the His protonation

Table 1
The residues found in the hydrogen bond network; Residues are divided by their properties: PT are capable of direct participation in Grotthuss proton transport or by being transiently protonated/deprotonated; Polar, non-Grotthuss: can make hydrogen bonds to anchor the network but are unlikely to carry a proton towards the lumen; Non-polar: residues associated with the channels that have been the subject of prior investigation [56,68,72,73]. Residues are also separated by their location: Origin: position on the OEC that is closest to the channel entrance; Interconnected near OEC: region including residues shown in Fig. 2B; Separated Channel: residues in the separated channel; Surface residues: residues with >20% surface exposure. *Primary ligands of the OEC. #Surface residues connected to multiple channels. The colors assigned to each channel are used in all figures. Recently the narrow, broad and large channels were referred to as O4, O5 and O1 channels, indicating the atoms in the OEC where they are proposed to originate [19].

Channel	Residue type	Origin	Interconnected near OEC	Separated channel	Surface residues
Narrow Magenta	PT	O4,Mn4-W1	D1-D59, S86, S169 [67], CP43-S310, H332*, E354*	D1-S85, S167 (near OEC), D1- H337, CP43-T335, T355, D321	PsbU-E93, D96, CP43-K339
	Polar non-Grotthuss		D1-N87 [68], N108, CP43-Q313, R357, PsbU-R97	D1- N338, CP43-Q311, PsbU-N31, N99, N100, D2-N350	
	Non-polar		D1-P334		
Broad Green	PT	O5,Mn4-W1, W2	D1-D61 [69], D2-K317 [30,70], PsbO-D99, D102, E333*	D1-S177, E65 [71], D2- E310, E312, D2- Y315§, T316, PsbO-E97, D99, D102 [42]	D2-D308, PsbO-D158, K188, D222, D223§, D224, H228, E229§
	Polar non-Grotthuss		D1-R64, N181, R334	D1-N335, D2-N318, PsbO-R152	
	Non-polar		D1-V185 [72]		
Large Orange	PT	O1, Ca—W3, W4	D1-Y161, D170*, E189*, D342*	D1- H190, E329, CP43- E83, E413, E394, T412, H398, K79, T397, PsbV- S39	PsbU-K47, K134, PsbV-K103, K104
	Polar non-Grotthuss			D1-Q165, Q187, N191, N296, N298 [56,73], N325, D2-R348§, CP43-N418	
	Non-polar		PsbV-L341		

and tautomeric states are modified based on the results of the MCCE simulation [58]. Non-standard ionization or tautomer choices are provided in SI S4. The total system charge is neutralized at an ionic strength of 0.15 M by the addition of 616 sodium and 320 chloride ions. The partial charges for the S_1 OEC including the primary ligands are derived with Gaussian [45]. Parameters for other cofactors are from the Bondar group [61]. The CHARMM [60] setup package is used to fix the bond connectivities for both heme and non-heme Fe. MD trajectories are run in OPENMM [62].

2.2. MCCE calculations

Multi-Conformation Continuum Electrostatics (MCCE) [58] calculations are carried out on 10 snapshots from the 100 ns S_1-state MD trajectory. Individual snapshots are chosen with the MDAnalysis clustering algorithm [63] and represent structural clusters based on the distances between D1-D61, E65, D2-E312, K317, PsbO-D224 and Cl^-. The calculations only include the 88 Å × 70 Å × 65 Å rectangular region containing the OEC and the regions of the protein that connect the OEC to the lumen (Fig. 1A, SI S1). All atoms outside the rectangular region are deleted. All lipids and water molecules that were surface exposed around the whole protein are removed.

MCCE [58] uses the continuum electrostatics program Delphi to calculate electrostatic energies from the Poisson-Boltzmann equation. The same methods and parameters used in previous studies of PSII are used here [29,30] and described in detail in SI S4B.

MCCE is always limited to a fixed backbone. Here we use iso-steric sampling, which finds the many hydrogen bond/protonation/tautomer states in a Boltzmann distribution consistent with the side chain carbon positions found in the input MD snapshot. Thus, the neutral and ionized protonation states of the Asp, Glu, Arg, Lys, His and Tyr residues are sampled. The O and N of the side chain amide of Asn and Gln can exchange and both neutral His tautomers are sampled. Hydroxyls of Ser, Thr and Tyr can reorient. Both chlorides, one near D2-K317 and other near D1-N338 and F339, are included in the calculations. The primary OEC ligands, D1-E189, D1-E333, D1-D342 and CP43-E354, are fixed in their ionized state while D1-H332 is neutral [30].

The MCCE calculation retains waters within the MD snapshots with <15% solvent accessible area. All waters surrounding the protein are replaced by implicit solvent. The positions of the OEC atoms are retained along with the oxygen positions of the four terminal water ligands (Fig. 1B, SI S1). The positions of water oxygens within the protein are taken from the input MD snapshot. Each can choose between 15 and 20 different proton positions in Monte Carlo (MC) sampling and can sample neutral H_2O and hydronium H_3O^+ conformers. Except for the terminal waters of the OEC, all water molecules can move into solution in MC sampling. We find in the average of all accepted microstates, 92% of the input waters from the MD snapshot remain bound in the protein, with few positions having no occupancy.

2.2.1. Hydrogen bond network analysis

MCCE hydrogen bond analysis focuses on the rectangular region around the OEC (Fig. 1A, SI S1). For each snapshot, the calculations sample ≈33 million microstates during MC sampling, giving the distribution of protonation states, water occupancy and polar hydrogen positions. These are analyzed to obtain the Boltzmann distribution of hydrogen bond connections.

The combined MCCE-network hydrogen bond analysis has previously been used to analyze proton transfer pathways in cytochrome *c* oxidase and complex I, and the same methods are used here [13,64]. Hydrogen bonds have a distance between the donor, hydrogen (D—H) and acceptor (A) of 1.2 Å–3.2 Å and an angle between D—H and A > 90°. The connection is counted if the proton acceptor and donor form a hydrogen bond in >0.1% of accepted microstates in the MCCE simulation starting with a given MD snapshot. Cytoscape [59] draws the network (Fig. 2C). Residues are nodes and each line indicates the formation of a hydrogen bond, either directly connecting two residues or via as many as four bridging waters. Longer water chains do not find additional connected residues. Residues connected by four waters can be as much as 10-13 Å apart.

2.2.2. Estimation of the energy of hydronium ring transfer through the water channels

The free energy of hydronium (i.e. the water proton affinity) is calculated at pH 7 in the three channels. Hydronium is always disfavored in the channel, so regions where it is at lower energy have a lower barrier for proton conduction. This calculation may be viewed as the Monte Carlo analog of a Potential of Mean Force (PMF) calculation in MD [65]. The OEC is fixed in the S_1 state where Mn1 and Mn4 are in the +3 oxidation state while Mn2 and Mn3 are +4. One water at a time is fixed to be hydronium and the position (but not the charge) of nearby residues and water are allowed to come to equilibrium. In the MCCE calculations, all Asp, Glu, Arg and Lys near the OEC are found to be ionized and His are neutral except residues: D1-H92, H337, CP43-H91, H398, PsbO-H228, and PsbU-H81. The reference energy adds the energy of hydronium in solution (13.2 kcal/mol at pH 7) to the total MCCE

Table 2
Example paths from each of the four OEC waters to each of the three channels.

	W1	W2	W3	W4
Narrow	X434,	X429, W1, X434,	P9578, E12, X429, W1, X434,	W3, W2, W1, X434,
	All paths:X425, X424, Z4, P6395, Z21, P5192, P4445, P5284, P431, P5049, K339			
Broad	X429,	X429,	P9578, E12, *X429*,	W3, P9578, E12, *X429*,
	All paths: X428, P7478, P4713, X417, P1211, P5017, P9096, P8101, D224			
	Alternate path1: X428, D61, P7478, P4713, E312, P9604, P2773, P1510, P9096, D224			
	Alternate path2:X428, D61, P7478, P4713, X524, E65, P2577, P8298, P6850, D224			
Large	X429, E12, P9578, W3, W4, *P9335*	X429, E12, P9578, W3, W4, *P9335*	W4, P9335,	P9335,
	All paths: P9335, **P2436**, P5108, P2656, P9584, P815, P6926, P8089, P3306, P6393, P9357, P4873, X447, P7214, P4347, P8277, K103			
	Alternate path1: **P2436**, P5108, E329, P815, P6926, P8089, P3306, P6393, P9357, P4873, X447, P7214, P4347, P8277, K103			
	Alternate path2: **P2436**, P5108, E329, P815, P6926, P8089, E413, P4677, P4873, X447, P7214, P4347, P8277, K103			

Representatives of the many connections through one snapshot of the inner region shown in Fig. 2B. Chain X, E and Z are water molecules obtained from the crystal structure and chain P are waters added during MD set up. Amino acids on the paths are underlined. Waters that are common to all paths along one channel are in italics.

energy of PSII relaxed without the hydronium. This is compared with the PSII energy with the hydronium in each position walking from the OEC to the lumen. Recent MCCE benchmark calculations of proton transfer in the gramicidin channel [65] found good agreement between the barrier for proton transfer estimated from the hydronium free energy and that obtained earlier using the higher level, Empirical Valence Bond (EVB) calculations [66]. The hydronium free energy is obtained at 8 ± 2 water positions in each water channel in 10 individual snapshots, comparing 240–300 positions.

3. Results and discussion

3.1. Analyzing the hydrogen bond network near the OEC

The OEC is ~20 Å from the lumen. In the work presented here the connections from the OEC to the surface are traced by combined MD/MC/Network Analysis. MD trajectories allow the protein to explore conformational space, while the MC analysis provides the Boltzmann distribution of hydrogen bonds (i.e., those that are energetically accessible), as well as residue protonation states, that are consistent with the heavy atom positions in individual input MD snapshots. Networks include all internal waters from the MD snapshot. As will be shown, the network is dominated by water molecules, but amino acid side chains play significant roles defining the water-filled channels.

3.2. Representations of the pathways from the OEC to the lumen

Fig. 2 shows the hydrogen bond network around the OEC. Residues and waters are colored by their assignment to a given channel (Table 1). Fig. 2A shows a conventional view of the polar residues and waters within 10 ± 2 Å of the OEC. This highlights the separation of the channels going away from the OEC. However, Fig. 2B shows the multiplicity of connections, largely through waters, within 10 ± 2 Å of the OEC, while Fig. 2C provides a more schematic view, with only the amino acids that are hydrogen bonded via waters reaching from the OEC to the lumen. Each figure will be shown to highlights the complexity of the possible pathway for a proton in different ways.

3.3. Protons released from any site on the OEC can enter any channel via interconnected waters

Fig. 2B shows the results of the network analysis of the hydrogen bonds found by MC sampling of the polar proton and water positions within 15 Å of the OEC in a single MD snapshot. The channels are well separated beyond 10–12 Å of the OEC and these will be described below. However, near the OEC there are numerous connections amongst waters anchored by residues. Thus, here the network is better described as a river delta than as three separate channels. Table 2 provides examples of several paths from each primary OEC water ligand to the lumen. Nominally W1 is identified with the narrow and broad channels, W2 with the broad channel, and W3 and W4 with the large channel. However, multiple paths can be found allowing a proton from each of the four terminal water ligands to exit via any of the three channels. The number of steps to reach a region where the channels are separated ranges from zero for W1 and W2 entering the broad channel or W4 to the large channel to five steps needed for W1 or W2 to enter the large channel.

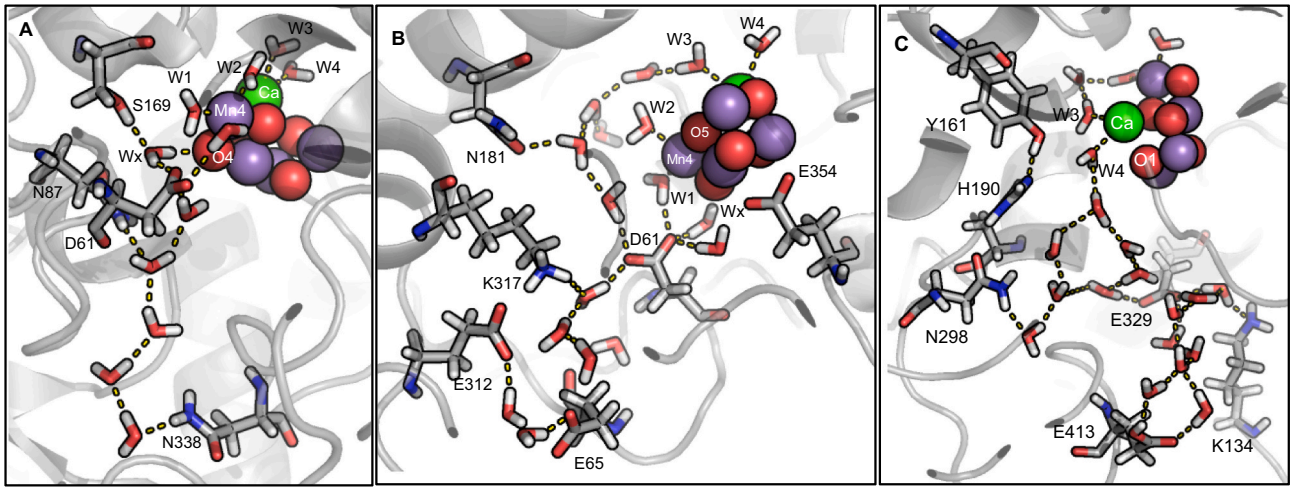

Fig. 3. Representative hydrogen bonding pathways via ordered waters in a single MD snapshot. (A) Near O4 leading towards the narrow channel showing D1-D61, N87, S169, N338 (B) Near O5 leading towards the broad channel showing D1-D61, E65, N181, D2-E312, K317 and CP43-E354; (C) Near O1 leading towards the large channel showing D1-Y161, H190, N298, E329, CP43-E413 and PsbV-K134.

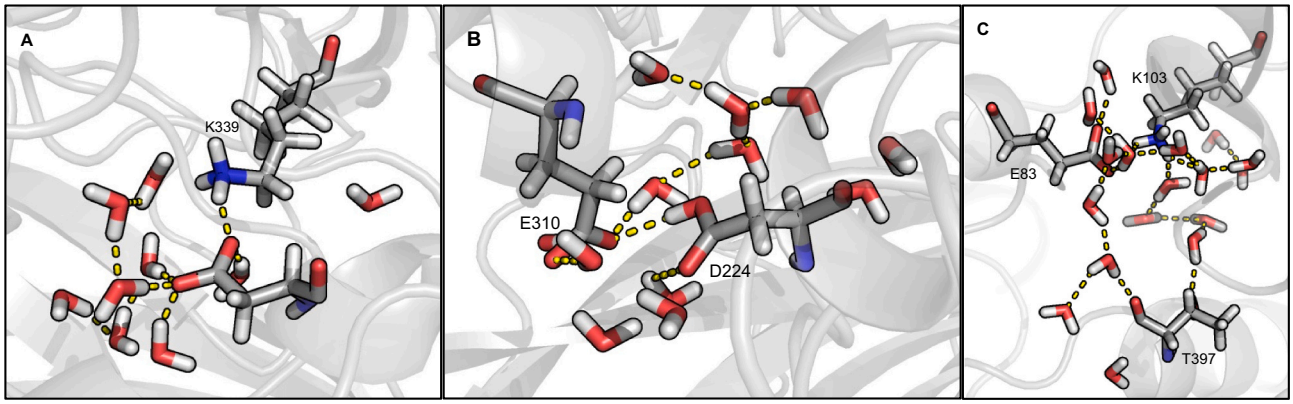

Fig. 4. Network of hydrogen bonds from a single MD snapshot showing pathways through separated channels. (A) Narrow channel showing CP43-K339 and PsbU-D96. (B) Broad channel showing D2-E310 and PsbO-D224. (C) Large channel showing CP43-E83, T397 and PsbV-K103.

3.4. The connections from the bridging oxygens in the OEC cluster

A proton is likely to be lost from one of the bridging oxygens in the S_0 to S_1 transition [3,24,26–28]. Fig. 3 shows that with modest remodeling of the hydrogen bond network a proton on O1, O4 or O5 can enter into the water-filled channels. However, the primary ligands create a boundary around O2 and O3, with the C-terminus D1-A344 blocking O2 and D1-H337 blocking O3, so they are poorly connected to the network.

3.5. Amino acid participation in the network near the OEC

Fig. 2B and Table 2 show the connections available for proton transfer in one snapshot. The connections are dominated by waters. As the individual water molecules exchange within the trajectory the table shows representative paths protons can take. Paths from the OEC to the lumen can be traced solely via waters without protons needing to hop though any amino acids. However, paths can also be drawn with protons transferring via protonation/deprotonation of D1-D61 and D2-E312 to the broad channel or via D1-E329 and CP43-E413 to the large channel.

Fig. 2C highlights the amino acid side chains making hydrogen bonds to waters within the channels. The network shown extends to the lumen. In the schematic network, a line connecting two residues can indicate anywhere from 0 to 4 intervening water molecules. The inner circle consists of the four water ligands, W1, W2, W3 and W4 at the center of the network. The four OEC water terminal ligands are surrounded by the six primary ligands. All primary ligands to the OEC Mn are connected to at least 6 other residues, sometimes directly but more often through complex water chains, with the exception of the Mn1 ligand D1-H332 which is isolated and only connected to H337. The next circle shows the residues near the OEC. While these are colored to indicate the channel with which they have been associated, they are interconnected by the complex water network shown in Fig. 2B. The outer circle shows the residues in the well separated channels and the surface residues (triangles) where protons can exit. The peripheral residues connected to the outer circles make few connections to other residues in the network and are often on the surface. Networks obtained with different snapshots are provided in Supplementary Material (SI S2). They are drawn with the same layout so they can be easily compared. Peripheral residues that are unconnected in the network shown in Fig. 2B are connected in the analysis starting with different MD snapshots. Overall, the network shows a total of 74 residues, with 23 residues identified in the broad channel, 26 residues in the narrow channel and 25 large channel residues (Table 1, Fig. 2C).

Fig. 2B and C shows the residues identified with each channel are linked near the OEC by multiple of possible connections. Different types of residues with different roles in proton transfer are found near the entry to each channel. Thus, the narrow channel has more hydroxyl, Grotthuss competent residues and only one acid; The broad channel has more potentially proton loading Asp and Glu as does the large channel. Each channel is identified with multiple Asn, which can anchor the network. We will give several examples that highlight the interconnections of residues that have been previously shown to effect oxygen evolution.

3.6. The connections via D61

D1-D61, which bridges the narrow and broad channels, is a direct hydrogen bond acceptor of W1 and W_X. D61 can help trap the proton being released from W1 as Mn4 is oxidized in the S_2 state [30]. In different conformations in the Boltzmann ensemble, W_X makes hydrogen bonds to the O4 μ-oxo bridge as well as to D1-S169 and the D61 carboxylate. These water molecules connect D61 to residues identified with the narrow channel residues D1-S169, N87, N335, CP43-R357 (Fig. 4A) and broad channel residues D1-N181, D1-R334, D2-K317 (Fig. 4B) as well as all four OEC water ligands. Thus, a large number of amino acid residues can be connected to D61 either directly or via waters without any intervening amino acids.

The D1-D61A mutation blocks the OEC from advancing beyond S_2. The mutation modifies the FTIR spectral changes between S_1 to S_2 and S_2 to S_3, supporting a role for this residue in the active proton transport network [69]. FTIR studies [74,75] find a large hydrogen bond network that includes D1-D61. For example, mutation of D1-E329, identified with the large channel, shows changes in the FTIR spectra similar to those associated with D1-D61 or with E65 and D2-E312 in the broad channel.

3.7. The connections near Y161(Y_Z)/H190

Y_Z is the electron donor to P_{680} and it in turn oxidizes the OEC. On oxidation it transfers its hydroxyl proton to H190. The connection between them is constrained in the MD trajectory (see SI S4). The hydrogen bond is seen in the network analysis. The few waters around the Y_Z/H190 pair are not well connected to the larger hydrogen bond network surrounding the OEC. The nearby N296 and N298 are not Grotthuss conducting residues. Thus, the network analysis suggests poor egress opportunities for a proton bound between Y_Z and H190. This is advantageous as the proton must not be lost from the His as it must return to the Tyr when the electron is transferred from the OEC to reduce Y_Z.

3.8. The connections via D2-K317

D2-K317, near D61, and the Cl^- bound near the OEC are associated with the broad channel (Fig. 3B). The Lys is connected to D61 via water molecules, and with D1-E65, N181, D2-E312 (broad channel) and with

D1-D59 (narrow channel) as well as with the primary ligands D1- E333, D170 and E189 and all four OEC water ligands. D2-K317A or K317R mutants show reduced O_2 evolution blocking/slowing advancement beyond S_2 [70,74]. Simulations have shown that in the absence of Cl^-, D61 and K317 form a salt bridge that can cut off the hydrogen bond network entering the broad channel [76].

3.9. The connections via D1-N181 and N87

D1-N181 is identified with the broad channel. It forms hydrogen bonds via waters to the primary ligands D1-D170, E189, E333 and CP43-E354 as well as to W2 of Mn4. The network analysis finds water mediated connection to D1-D61, D2-E312, K317 (broad channel), to D1-D59, S169, CP43-R357 (narrow channel) and to D1-Q165 (large channel). An Asn is unlikely to directly participate in proton transport but can play a role in anchoring the hydrogen bond network. With the rotation of the terminal amide, the side chain can reorient the direction of its hydrogen bond donor and acceptor ends. MCCE finds this Asn to be oriented with the NH_2, proton donating side, oriented towards D1-D61. FTIR studies on N181A mutated PSII [74,77] found that this residue is part of the hydrogen bond network that includes D1-D61 described above.

D1-N87, which is identified with the narrow channel, forms water mediated hydrogen bonds to D1-S167, S169, N338, CP43-T335 and R357 (narrow channel), with D1-D61 (broad channel) and with the primary OEC ligands D1-E333, D170, CP43-E354 and W1 and W2. FTIR difference spectra [68] of D1-N87A mutated PSII look like those found for the wild-type PSII, although flash-induced O_2 evolution studies do show a decrease in the cycling efficiency.

3.10. The connections via CP43-R357 and D1-R334

CP43-R357 is associated with the narrow channel. The guanidinium group can donate as many as five hydrogen bonds to widely spaced waters or residues. The Arg forms hydrogen bond connections via waters to D1-N87 (narrow channel), D1-D61 and N181(broad channel) and D1-Y161 (large channel), as well as to the primary ligands D1-E333, D170, E189, CP43-E354 and to the OEC water ligands. FTIR studies [74,78] find that R357 participates in a hydrogen bond network with the Ca and Mn water ligands. Previously, it was proposed [79] that this residue may be involved in proton transfer to the lumen beyond the S_2 state. However, Arg has a very high intrinsic proton affinity so is unlikely to become deprotonated in the protein [80].

R334 is associated with the broad channel. The network analysis finds D1-R334 hydrogen bonded to residues D1-D59, D61, E65, D2-E310, E312 and T316 (broad channel). Mutation of this residue finds changes in the efficiency of the S-state transitions beyond S_1 including the S_3 to S_0 transition. FTIR spectra [81] on D1-R334A PSII shows the elimination of C═O peaks in S_2-S_1 and S_3-S_2 difference spectra.

4. Hydrogen bond network moving away from the OEC near to the lumen via the three water channels

4.1. Characterization of the channels away from the OEC

The network analysis shows two regions, one where the network is highly interconnected near the OEC followed by well separated channels moving to the lumen. Roughly the large channel separates near Cδ of D1-E329 10.6 Å from the OEC Ca; the narrow channel entrance is near Oγ of D1-S169, 6.4 Å from Mn4; the broad channel separates from the interconnected region near Cδ of D1-E65, 13.6 Å from Mn4.

4.2. Connection to the lumen via the narrow channel

The network analysis shows D1-S169, in the highly interconnected region, connects to D1-N338, in the separated narrow channel, by a linear chain of ~6 water molecules (Fig. 3A). QM/MM calculations also found a well ordered water chain from O4 to D1-N338 [82]. Moving outward, D1-N338 and CP43-T335 are connected via 4 waters. Thus, the narrow channel is indeed narrow. It exits to the lumen near PsbU-E93, D96, CP43-K339 (Fig. 4A).

On the surface, there are many hydrogen bond connections near the narrow channel exit. CP43-K339 and PsbU-D96 are connected as a salt bridge. CP43-K339 is at the center of a water mediated network connecting PsbU-E93 and CP43-T335 and anchored by D1-N338 and PsbU-N99. The water mediated network also connects PsbU-N99 with CP43-D321 and PsbU-E93 with PsbO-D102 (SI S2). PsbO-D102 is near the broad channel exit.

4.3. Connection to the lumen via the broad channel

The broad channel separates from the region around the OEC close to the narrow channel entry, with D1-D61 associated with both channels. D1-E65, D2-E310 and E312 are at the boundary between the highly interconnected region near the OEC and the channel proper (Fig. 3B). Moving along the broad channel we find D1-S177, D2-N318, D2-T316, PsbO- R152, D102, D99. The broad channel exits to the lumen through PsbO-D158, K188, D224, D222 and H228 (Fig. 2C). These residues extend over 10 Å and are connected via clusters of waters. FTIR difference spectra support many of these residues being part of a long range hydrogen bond network [71].

Previous studies have analyzed the multiple clusters of Asp and Glu residues on the surface of PsbO near the broad channel exit which can serve as proton loading sites [42]. These are connected either by direct hydrogen bonds or via water molecules [42]. For instance, D2-E310 is at the center of a surface network connected to the acids PsbO-D222 and D224, and the bases H228 and K188 (Fig. 2C and Fig. 4B). There is a direct hydrogen bond trapping a proton between two acids PsbO-D102 and E97 as noted previously [42].

4.4. Connection to the lumen via the large channel

D1-E329 can be viewed as the boundary between the highly interconnected region near the OEC and the large channel, which runs through CP43 and PsbV. Although the large channel has been considered to be less polar, CP43- E413, T397, H398, PsbV-S39, E83, K79 are in the large channel water mediated network. The channel exits to the surface near the bases PsbV-K103, K104 and K134. PsbV-K103, which forms a salt bridge with CP43-E83, is at the center of a network that includes residues CP43- T397, E394, and H398 (Figs. 2C and 4C).

4.5. Interconnections between the channels at their exits

The large channel exits to a well separated region of PsbU and PsbV. In contrast, the narrow and broad channel entrances are near each other and their exits are interconnected by residues in PsbO and PsbU in an extended surface network. These surface connections are flexible and vary between MD snapshots. For example, transient connections are found between PsbU-E93 (narrow channel) and PsbO-D102 (broad channel) in the MD trajectory (Fig. 2C).

4.6. Continuity of hydrogen bond connections with the channels

The network analysis shows that rather than starting out as three independent water channels, the pathways are highly interconnected by many waters near the OEC (Fig. 2B and C, SI S2). The MD trajectories allow the mobility of these waters to be assessed. With the exception of W_X, which is directly hydrogen bonded to O4, all other waters in the interconnected area around the OEC are found to leave and be replaced by other water molecules during the 100 ns trajectory. Thus, despite their individual mobility, this water-mediated hydrogen bond network is very stable overall.

The network analysis compared the persistence of hydrogen bonded

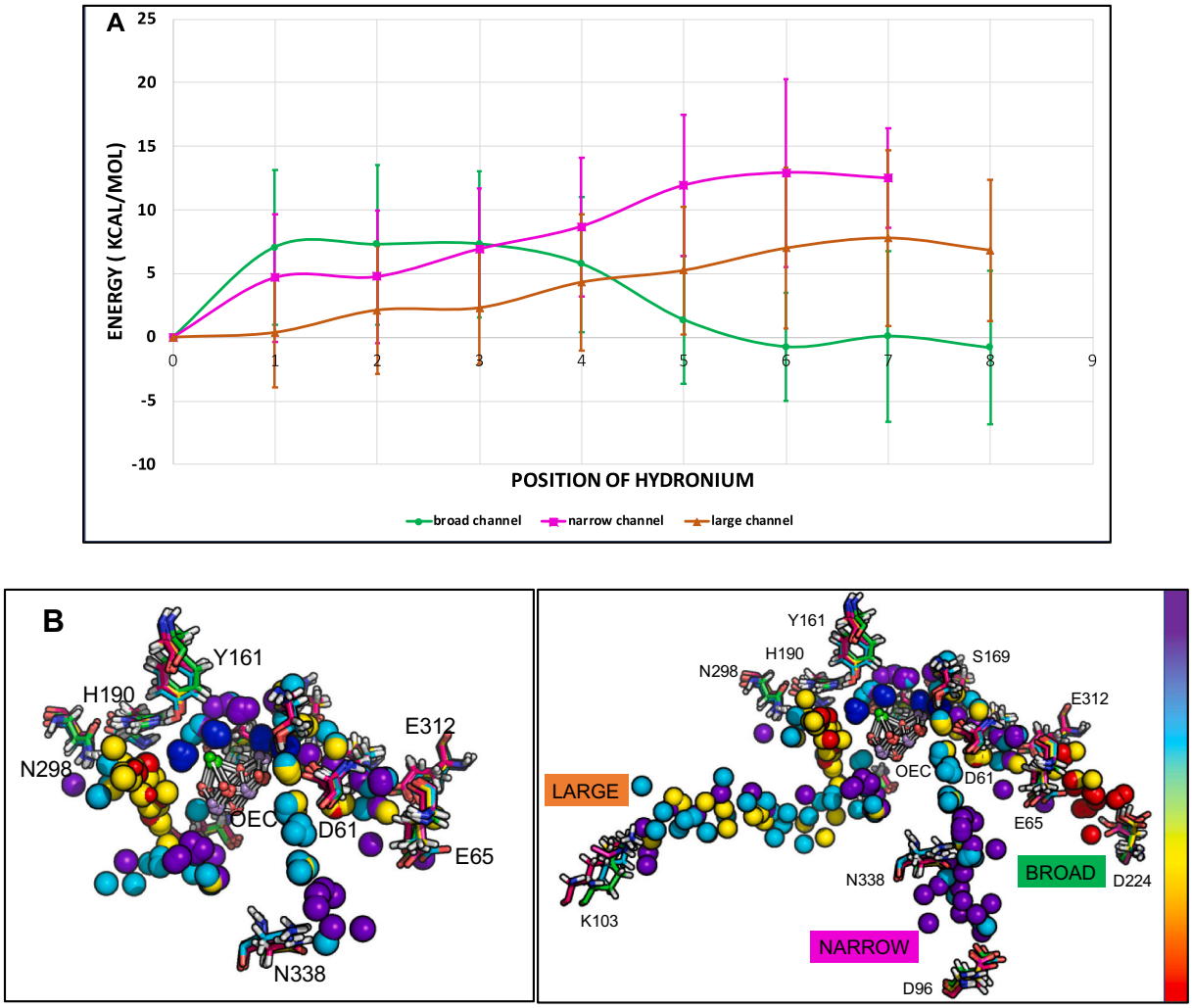

Fig. 5. **(A)** Energy of PSII in MC sampling with hydronium at different positions moving into and along the broad, narrow and large channels. The average values from ten snapshots are shown with standard deviation shown as error bars. The reference energy (at position 0) is for the full protein with no hydronium plus the energy of an isolated hydronium in water at pH 7. The amino acids near each position are described in the text. Orange: Large channel; Magenta: narrow channel; Green: broad channel.
(B) Energy landscape for water molecules near the OEC (**left**) and reaching to the lumen (**right**) for all the waters in the channels. The results from ten MD snapshots are superimposed. The water oxygens are colored to show the relative energy of the protein with hydronium with red<yellow<cyan<purple. Red is the most favorable and each color represents a 5 kcal/mol energy range. D1-D61, E65 and D2-E312, PsbO-D224 (broad channel), D1-S169, N338, PsbU-D96 (narrow channel) and D1-H190, Y161, N298 and PsbV-K103 (large channel) are shown. Fig. SI S3 shows energy plots for individual snapshots.

connections in multiple MD snapshots in the separated channels moving towards the lumen. The broad channel forms a long, unbroken hydrogen bond pathway in 90% of the snapshots, while the narrow and large channels each become disconnected near the lumen in 30–40% of the snapshots. The break in the narrow channel occurs near CP43-K339 while for large channel, the hydrogen bond connection gets broken near PsbV-S39 and K103. In each case the connections are broken by transient dehydration events.

4.7. Proton affinity and protonation states of acidic and basic residues

MCCE keeps the protonation states of all amino acids in equilibrium with the pH and the hydrogen bond network. Most acidic and basic residues in the region around the OEC retain their expected protonation states. However, earlier MCCE studies identified some residues with different equilibrium ionization in the S_1 state and these are fixed in the MD trajectories [30] (See SI S4). All residues except for the primary amino acid ligands of the OEC are free to take any protonation state in the MCCE network analysis.

There are numerous acidic and basic residues within the highly interconnected region near the OEC (Table 1). Previous calculations of the proton affinity of residues in this region showed D1-D61, E65 and E329, which are well connected to the network; each has a significantly higher proton affinity than Asp or Glu in solution, although they are all predominantly anionic at pH 6 [10,30]. The higher proton affinity diminishes the free energy needed to transiently bind protons entering the broad channel. The higher proton affinity for the acids indicates an environment that will also be less unfavorable for hydronium. Earlier continuum electrostatics based calculations [10] found the pK_as of D1-D61, E65, D2-E312, D2-K317, D59, R64, PsbO-R152 and D224 increase moving outward in the broad channel, supporting their ability to function as proton loading sites.

4.8. Relative energy of hydronium in the water networks

The three channels are all interconnected near the OEC (Fig. 2B and C) and multiple proton transfer pathways to the lumen can be identified for any proton (Table 2). The relative energy of a positive charge will

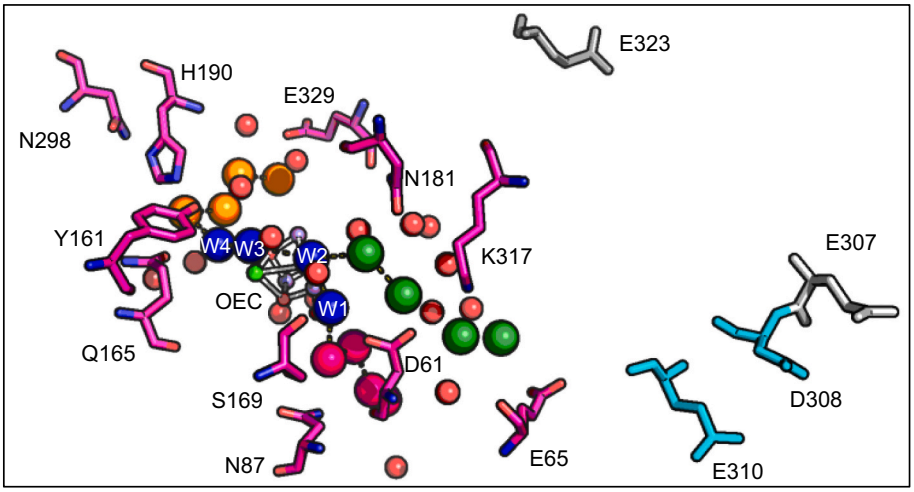

Fig. 6. Residues identified as being members of a long-range hydrogen bond network by FTIR difference spectroscopy. The residues are: D1- D61 [69], E65 [71], N181 [74,77], D2-K317 [70] (broad channel): D1-N87 [68], S169 [67] (narrow channel): D1-Y161 [85], H190, Q165 [81], N298 [73], E329 [71] (large channel). Residues and waters are colored for the channel with which they are most closely associated as described for earlier figures; Cyan and Grey: residues whose mutation does not alter the FTIR difference spectra. Cyan: D2-E310, D308 are connected to the end of the broad channel in the MCCE derived network; Grey: D2-E307 and E323 are not in MCCE network. Note that D2-E323 is on the surface and is farther away from D2-K317 than it appears in the figure.

play a role in deciding which path is taken. The free energy of replacing each water with a hydronium was determined in MCCE. In each of the 10 snapshots the energy of hydronium is obtained at 7–8 locations in each of the three channels moving from the OEC to the lumen. The surrounding water molecules and amino acid residues are allowed to reorient to stabilize the H_3O^+ but not change charge or leave the protein. Fig. 5A shows the average hydronium energy at comparable positions in the 10 snapshots. We do not wish to suggest a hydronium proper is moving through the channel. Rather in a Grotthuss proton transfer mechanism each water in the chain is transiently associated with a the proton. Thus, these calculations should be viewed as probing the relative energy of a positive charge moving through the network via waters or amino acids [10].

Fig. 5A shows the averaged energy at eight locations from ten superimposed snapshots, chosen by meta-analysis of the trajectory. The reference energy (position 0) is the sum of the energy of the protein (without hydronium) plus that of hydronium in solution. To differentiate the channels in the intertwined network near the OEC, the broad channel is considered to start near the waters of Mn4 moving towards PsbO-D224, while the narrow channel starts near D1-S169 moving towards CP43-K339 and PsbU-D96 and the large channel starts near Ca moving towards the PsbV-K103.

Fig. 5B colors the relative energy of each water in each superimposed snapshot to provide a qualitative picture. Here the hydronium energy, which varies from 0 to 20 kcal, is binned into four 5-kcal groups, with the proton affinity decreasing from red to yellow to cyan to purple. Regions more favorable for hydronium (red and yellow) remain distinct from those that are less hospitable (cyan and purple).

Moving along the narrow channel, positions 1, 2 and 3 (yellow and cyan in Fig. 5B) are near D1-S169 and D1-D61. The less favorable positions 4 and 5 (cyan and purple) are close to D1-N338 and CP43-T335; unfavorable energy is found near positions 6 and 7 (cyan and purple) close to CP43-K339 and D1-D96. Dehydration events in the MD trajectory take place near position 6. Thus, although the region of the interconnected network close to the narrow channel is favorable for a positive charge, the channel itself is not.

In the broad channel, positions 1 and 2 (cyan and purple), near D1-V185 are relatively unfavorable for hydronium compared to positions 3 and 4 (yellow and cyan) near D1-N181 and D61. Positions 5, 6, 7 near D1-E65 and D2-E312 (yellow and red) and 8 (red) near PsbO-D224 are relatively favorable for a positive charge, showing the reduction of the barrier for a proton moving along the broad channel [10].

Tracing hydronium through the large channel shows a favorable region at positions 1–3 (yellow and red) near the neutral D1-H190, N298, D1-D342, D1-Q165 and W4. This region, near Y_Z may help stabilize the buildup of charge when it is transiently oxidized. However, moving outward the free energy of the hydronium probe increases. Positions 4, 5 and 6 are near D1-E329 and CP43-E413 (yellow, cyan and purple) while 7 and 8 are near the channel exit PsbV-K103 (cyan and purple). The dehydration of the large channel occurs near position 7.

The relative energy for hydronium near to OEC in all the water channels are within the error bars. More favorable positions are at W_X near to D1-S169 in the narrow channel, at waters near D1-N298 in the large channel and waters near D1-D61 in the broad channel (Fig. 5B). However, as the protons move away from the OEC, the energy is more favorable in the broad channel while it continually increases moving through the narrow and large channels. Thus, the broad channel will lower the energy of a proton moving towards the exit, while the energy increases moving towards the exit of the other channels.

4.9. Comparison of network analysis results with network proposed by FTIR

FTIR spectra are very sensitive to protonation states and hydrogen bond strengths in networks of waters and amino acids. As a raw FTIR spectrum is extremely congested, the difference between spectra in different S-states, and double difference spectra comparing wild-type protein with that labeled with different isotopes or modified by site-directed mutations are used to probe the network that responds to the OEC reactions. Many mutations have been made in the region of amino acids separated by as much at 20 Å around the OEC shown in Fig. 6. These include: the large channel residues D1-Q165E [81], D1-E329Q [71], N298A [73], narrow channel residues D1-N87A [68], D1-S169A [67,83] and broad channel residues D1-D61A [69], E65A [71], N181A [74,77] and D2-K317A, K317R, K317Q, K317E [70,84]. It was found that mutations of the residues in the inner, interconnected network described here produce similar changes in OEC function as well as in the FTIR signatures of the hydrogen bond networks [71,74].

Mutations of D2-E307; D2-D308; D2-E310 and D2-E323 do not modify the FTIR spectrum [81]. D2-E310 and D2-D308 are in the MCCE network, but the former is near the end of the broad channel and the later on the surface. D2-E307 and E323 are not connected to the network found here, nor do their mutation affect the FTIR difference spectra (highlighted in grey color) (Table 1).

5. Conclusions

The results characterize the full proton egress pathway by combined classical MD, MCCE and network analysis. An unexpected conclusion is that the three channels are highly interconnected in a region reaching 10 ± 2 Å from the edge of the OEC (Fig. 2B). In addition, the free energy of a hydronium probe replacing all of the waters around the OEC is

similar at most sites in this region, independent of which is the nearest channel entry. The three channels do disentangle themselves as they move towards the lumen. However, the entries to the narrow and broad channels are close together near the OEC, connected by D61 and they are also interconnected by surface hydrogen bond networks at their exits.

The results reported here support the broad channel as the preferred proton exit. It retains a lower, energy for hydronium to the end of the channel (Fig. 5B). This is in agreement with earlier continuum electrostatics studies for only this channel [10] that used the pK_a's of amino acids as a probe, showing increasing proton affinity moving along the broad channel to the lumen. In contrast, the energy of the hydronium probe in the narrow and large channels increases moving towards the exit. Additionally, the broad channel water chains are rarely broken in the MD trajectory, while the narrow and large channels become transiently disconnected by dehydration events. This result supports earlier MD simulations that found a long-range hydrogen bond network starting from Mn4 of the OEC extending to the PsbO subunit present in the lumen through the broad channel [10,12,42].

Declaration of competing interest

The authors declare that they have no known competing financial interests or personal relationships that could have appeared to influence the work reported in this paper.

Acknowledgements

We would like to acknowledge Dongyue Liu from Boston University for insightful discussions and assistance in the set-up of the PSII MD calculations in CHARMM and OpenMM. The authors would like to acknowledge financial support from the Division of Chemical Sciences, Geosciences, and Biosciences, Office of Basic Energy Sciences, U.S. Department of Energy, Photosynthetic Systems. Experimental work was funded by DESC0001423 (M.R.G. and V.S.B.) and DE-FG02-05ER15646 (G.W.B.). V.S.B. acknowledges DOE high-performance computing time from NESRC. The MD simulations on monomeric PSII used the computing time from Memorial Sloan Kettering Cluster and resources at Oak Ridge National Laboratory, supported by the Office of Science at DOE under the contract no. DE-AC05-00OR22725, made available via the INCITE program.

Appendix A. Supplementary data

S1 is a figure of PSII highlighting the portion of protein used for MCCE calculations, S2: Water mediated hydrogen bond network for nine representative snapshots, S3: Energetic profile for hydronium moving through the three channels in ten representative snapshots, S4:. Details of the PSII molecular dynamics and MCCE simulations setup, S5: Motion of water and chloride molecules observed in MD trajectory. Supplementary data to this article can be found online at doi:https://doi.org/10.1016/j.bbabio.2021.148446.

References

[1] N. Cox, D.A. Pantazis, F. Neese, W. Lubitz, Biological water oxidation, Acc. Chem. Res. 46 (2013) 1588–1596.
[2] D.J. Vinyard, G.W. Brudvig, Progress toward a molecular mechanism of water oxidation in photosystem II, Annu. Rev. Phys. Chem. 68 (2017) 101–116.
[3] D.A. Pantazis, Missing pieces in the puzzle of biological water oxidation, ACS Catal. 8 (2018) 9477–9507.
[4] Y. Umena, K. Kawakami, J.-R. Shen, N. Kamiya, Crystal structure of oxygen-evolving photosystem II at a resolution of 19 Å, Nature 473 (2011) 55–60.
[5] B. Kok, B. Forbush, M. McGloin, Cooperation of charges in photosynthetic O_2 evolution-I a linear four step mechanism, Photochem. Photobiol. 11 (1970) 457–475.
[6] M. Suga, F. Akita, K. Yamashita, Y. Nakajima, G. Ueno, H. Li, T. Yamane, K. Hirata, Y. Umena, S. Yonekura, L.-J. Yu, H. Murakami, T. Nomura, T. Kimura, M. Kubo, S. Baba, T. Kumasaka, K. Tono, M. Yabashi, H. Isobe, et al., An oxyl/oxo mechanism for oxygen-oxygen coupling in PSII revealed by an x-ray free-electron laser, Science 366 (2019) 334–338.
[7] M.R. Gunner, M. Amin, X. Zhu, J. Lu, Molecular mechanisms for generating transmembrane proton gradients, Biochim. Biophys. Acta Bioenerg. 1827 (2013) 892–913.
[8] A. Gabdulkhakov, A. Guskov, M. Broser, J. Kern, F. Müh, W. Saenger, A. Zouni, Probing the accessibility of the Mn_4Ca cluster in photosystem II: channels calculation, noble gas derivatization, and cocrystallization with DMSO, Structure 17 (2009) 1223–1234.
[9] F.M. Ho, S. Styring, Access channels and methanol binding site to the $CaMn_4$ cluster in photosystem II based on solvent accessibility simulations, with implications for substrate water access, Biochim. Biophys. Acta 1777 (2008) 140–153.
[10] H. Ishikita, W. Saenger, B. Loll, J. Biesiadka, E.-W. Knapp, Energetics of a possible proton exit pathway for water oxidation in photosystem II, Biochemistry 45 (2006) 2063–2071.
[11] S. Vassiliev, T. Zaraiskaya, D. Bruce, Exploring the energetics of water permeation in photosystem II by multiple steered molecular dynamics simulations, Biochim. Biophys. Acta Bioenerg. 1817 (2012) 1671–1678.
[12] L. Vogt, D.J. Vinyard, S. Khan, G.W. Brudvig, Oxygen-evolving complex of photosystem II: an analysis of second-shell residues and hydrogen-bonding networks, Curr. Opin. Chem. Biol. 25 (2015) 152–158.
[13] X. Cai, K. Haider, J. Lu, S. Radic, C.Y. Son, Q. Cui, M.R. Gunner, Network analysis of a proposed exit pathway for protons to the P-side of cytochrome c oxidase, Biochim. Biophys. Acta Bioenerg. 1959 (10) (2018) 997–1005.
[14] M. Wikström, V. Sharma, V.R.I. Kaila, J.P. Hosler, G. Hummer, New perspectives on proton pumping in cellular respiration, Chem. Rev. 115 (2015) 2196–2221.
[15] C.J.T. de Grotthuss, Memoir on the decomposition of water and of the bodies that it holds in solution by means of galvanic electricity 1805, Biochim. Biophys. Acta 1757 (2006) 871–875.
[16] S. Hammes-Schiffer, E. Hatcher, H. Ishikita, J.H. Skone, A.V. Soudackov, Theoretical studies of proton-coupled electron transfer: models and concepts relevant to bioenergetics, Coord. Chem. Rev. 252 (2008) 384–394.
[17] K. Brejc, T.K. Sixma, P.A. Kitts, S.R. Kain, R.Y. Tsien, M. Ormö, S.J. Remington, Structural basis for dual excitation and photoisomerization of the Aequorea victoria green fluorescent protein, Proc. Natl. Acad. Sci. U. S. A. 94 (1997) 2306–2311.
[18] G. Hummer, M. Wikström, Molecular simulation and modeling of complex I, Biochim. Biophys. Acta Bioenerg. 1857 (2016) 915–921.
[19] J. Kern, R. Chatterjee, I.D. Young, F.D. Fuller, L. Lassalle, M. Ibrahim, S. Gul, T. Fransson, A.S. Brewster, R. Alonso-Mori, R. Hussein, M. Zhang, L. Douthit, C. de Lichtenberg, M.H. Cheah, D. Shevela, J. Wersig, I. Seuffert, D. Sokaras, E. Pastor, et al., Structures of the intermediates of Kok's photosynthetic water oxidation clock, Nature 563 (2018) 421–425.
[20] M. Askerka, G.W. Brudvig, V.S. Batista, The O_2-evolving complex of photosystem II: recent insights from quantum mechanics/molecular mechanics (QM/MM), extended X-ray absorption fine structure (EXAFS), and femtosecond X-ray crystallography data, Acc. Chem. Res. 50 (2017) 41–48.
[21] C.J. Kim, R.J. Debus, Evidence from FTIR difference spectroscopy that a substrate H_2O molecule for O_2 formation in photosystem II is provided by the Ca ion of the catalytic Mn_4CaO_5 cluster, Biochemistry 56 (2017) 2558–2570.
[22] T. Lohmiller, V. Krewald, A. Sedoud, A.W. Rutherford, F. Neese, W. Lubitz, D. A. Pantazis, N. Cox, The first state in the catalytic cycle of the water-oxidizing enzyme: identification of a water-derived μ-Hydroxo bridge, J. Am. Chem. Soc. 139 (2017) 14412–14424.
[23] V. Krewald, M. Retegan, N. Cox, J. Messinger, W. Lubitz, S. DeBeer, F. Neese, D. A. Pantazis, Metal oxidation states in biological water splitting, Chem. Sci. 6 (2015) 1676–1695.
[24] R. Pal, C.F. Negre, L. Vogt, R. Pokhrel, M.Z. Ertem, G.W. Brudvig, V.S. Batista, S_0-state model of the oxygen-evolving complex of photosystem II, Biochemistry 52 (2013) 7703–7706.
[25] P.E.M. Siegbahn, Water oxidation mechanism in photosystem II, including oxidations, proton release pathways, O—O bond formation and O_2 release, Biochim. Biophys. Acta Bioenerg. 1827 (2013) 1003–1019.
[26] K. Saito, A.W. Rutherford, H. Ishikita, Energetics of proton release on the first oxidation step in the water-oxidizing enzyme, Nat. Commun. 6 (2015) 8488.
[27] T. Shimizu, M. Sugiura, T. Noguchi, Mechanism of proton-coupled Electron transfer in the S_0-to-S_1 transition of photosynthetic water oxidation as revealed by time-resolved infrared spectroscopy, J. Phys. Chem. B 122 (2018) 9460–9470.
[28] M. Yamamoto, S. Nakamura, T. Noguchi, Protonation structure of the photosynthetic water oxidizing complex in the S_0 state as revealed by normal mode analysis using quantum mechanics/molecular mechanics calculations, Phys. Chem. Chem. Phys. 22 (2020) 24213–24225.
[29] M. Amin, L. Vogt, W. Szejgis, S. Vassiliev, G.W. Brudvig, D. Bruce, M.R. Gunner, Proton-coupled electron transfer during the S-state transitions of the oxygen-evolving complex of photosystem II, J. Phys. Chem. B 119 (2015) 7366–7377.
[30] D. Kaur, W. Szejgis, J. Mao, M. Amin, K.M. Reiss, M. Askerka, X. Cai, U. Khaniya, Y. Zhang, G.W. Brudvig, V.S. Batista, M.R. Gunner, Relative stability of the S_2 isomers of the oxygen evolving complex of photosystem II, Photosynth. Res. 141 (2019) 331–341.
[31] J. Lavergne, W. Junge, Proton release during the redox cycle of the water oxidase, Photosynth. Res. 38 (1993) 279–296.
[32] H. Suzuki, M. Sugiura, T. Noguchi, Monitoring proton release during photosynthetic water oxidation in photosystem II by means of isotope-edited infrared spectroscopy, J. Am. Chem. Soc. 131 (2009) 7849–7857.

[33] P.E.M. Siegbahn, Mechanisms for proton release during water oxidation in the S_2 to S_3 and S_3 to S_4 transitions in photosystem II, Phys. Chem. Chem. Phys. 14 (2012) 4849–4856.

[34] N. Cox, J. Messinger, Reflections on substrate water and dioxygen formation, Biochim. Biophys. Acta 1827 (2013) 1020–1030.

[35] M. Amin, D. Kaur, K.R. Yang, J. Wang, Z. Mohamed, G.W. Brudvig, M.R. Gunner, V. Batista, Thermodynamics of the S_2 to S_3 state transition of the oxygen-evolving complex of photosystem II, Phys. Chem. Chem. Phys. 21 (2019) 20840–20848.

[36] C.J. Kim, R.J. Debus, One of the substrate waters for O_2 formation in photosystem II is provided by the water-splitting Mn_4CaO_5 Cluster's Ca^{2+} ion, Biochemistry 58 (2019) 3185–3192.

[37] M. Askerka, D.J. Vinyard, G.W. Brudvig, V.S. Batista, NH_3 binding to the S_2 state of the O_2-evolving complex of photosystem II: analogue to H_2O binding during the $S_2 \rightarrow S_3$ transition, Biochemistry 54 (2015) 5783–5786.

[38] J. Wang, M. Askerka, G.W. Brudvig, V.S. Batista, Crystallographic data support the carousel mechanism of water supply to the oxygen-evolving complex of photosystem II, ACS Energy Lett. 2 (2017) 2299–2306.

[39] I. Ugur, A.W. Rutherford, V.R.I. Kaila, Redox-coupled substrate water reorganization in the active site of photosystem II—the role of calcium in substrate water delivery, Biochim. Biophys. Acta Bioenerg. 1857 (2016) 740–748.

[40] M. Askerka, J. Wang, D.J. Vinyard, G.W. Brudvig, V.S. Batista, S_3 state of the O_2-evolving complex of photosystem II: insights from QM/MM, EXAFS, and femtosecond X-ray diffraction, Biochemistry 55 (2016) 981–984.

[41] T. Noguchi, FTIR detection of water reactions in the oxygen-evolving Centre of photosystem II, Philos. Trans. R. Soc. Lond. Ser. B Biol. Sci. 363 (2008) 1189–1195.

[42] A.-N. Bondar, H. Dau, Extended protein/water H-bond networks in photosynthetic water oxidation, Biochim. Biophys. Acta Bioenerg. 1817 (2012) 1177–1190.

[43] L. Kemmler, M. Ibrahim, H. Dobbek, A. Zouni, A.-N. Bondar, Dynamic water bridging and proton transfer at a surface carboxylate cluster of photosystem II, Phys. Chem. Chem. Phys. 21 (2019) 25449–25466.

[44] S. Lorch, S. Capponi, F. Pieront, A.-N. Bondar, Dynamic carboxylate/water networks on the surface of the PsbO subunit of photosystem II, J. Phys. Chem. B 119 (2015) 12172–12181.

[45] K. Reiss, U.N. Morzan, A.T. Grigas, V.S. Batista, Water network dynamics next to the oxygen-evolving complex of photosystem II, Inorganics 7 (2019) 39.

[46] T. Lohmiller, V. Krewald, M.P. Navarro, M. Retegan, L. Rapatskiy, M.M. Nowaczyk, A. Boussac, F. Neese, W. Lubitz, D.A. Pantazis, N. Cox, Structure, ligands and substrate coordination of the oxygen-evolving complex of photosystem II in the S_2 state: a combined EPR and DFT study, Phys. Chem. Chem. Phys. 16 (2014) 11877–11892.

[47] M. Mandal, M. Askerka, G. Banerjee, M. Amin, G.W. Brudvig, V.S. Batista, M. R. Gunner, Characterization of ammonia binding to the second coordination shell of the oxygen-evolving complex of photosystem II, Dalton Trans. 46 (2017) 16089–16095.

[48] D.A. Marchiori, P.H. Oyala, R.J. Debus, T.A. Stich, R.D. Britt, Structural effects of ammonia binding to the Mn_4CaO_5 cluster of photosystem II, J. Phys. Chem. B 122 (2018) 1588–1599.

[49] P.H. Oyala, T.A. Stich, R.J. Debus, R.D. Britt, Ammonia binds to the dangler manganese of the photosystem II oxygen-evolving complex, J. Am. Chem. Soc. 137 (2015) 8829–8837.

[50] M. Pérez Navarro, W.M. Ames, H. Nilsson, T. Lohmiller, D.A. Pantazis, L. Rapatskiy, M.M. Nowaczyk, F. Neese, A. Boussac, J. Messinger, W. Lubitz, N. Cox, Ammonia binding to the oxygen-evolving complex of photosystem II identifies the solvent-exchangeable oxygen bridge (μ-oxo) of the manganese tetramer, Proc. Natl. Acad. Sci. U. S. A. 110 (2013) 15561–15566.

[51] J. Schraut, M. Kaupp, On ammonia binding to the oxygen-evolving complex of photosystem II: a quantum chemical study, Chemistry 20 (2014) 7300–7308.

[52] P.H. Oyala, T.A. Stich, J.A. Stull, F. Yu, V.L. Pecoraro, R.D. Britt, Pulse electron paramagnetic resonance studies of the interaction of methanol with the S_2 state of the Mn_4O_5Ca cluster of photosystem II, Biochemistry 53 (2014) 7914–7928.

[53] M. Retegan, D.A. Pantazis, Interaction of methanol with the oxygen-evolving complex: atomistic models, channel identification, species dependence, and mechanistic implications, Chem. Sci. 7 (2016) 6463–6476.

[54] M. Shoji, H. Isobe, K. Yamaguchi, QM/MM study of the S_2 to S_3 transition reaction in the oxygen-evolving complex of photosystem II, Chem. Phys. Lett. 636 (2015) 172–179.

[55] E.M. Sproviero, J.A. Gascón, J.P. McEvoy, G.W. Brudvig, V.S. Batista, Quantum mechanics/molecular mechanics study of the catalytic cycle of water splitting in photosystem II, J. Am. Chem. Soc. 130 (2008) 3428–3442.

[56] M. Chrysina, J.C. de Mendonça Silva, G. Zahariou, D.A. Pantazis, N. Ioannidis, Proton translocation via tautomerization of Asn298 during the S_2-S_3 state transition in the oxygen-evolving complex of photosystem II, J. Phys. Chem. B 123 (2019) 3068–3078.

[57] S. Luber, I. Rivalta, Y. Umena, K. Kawakami, J.-R. Shen, N. Kamiya, G.W. Brudvig, V.S. Batista, S_1-state model of the O_2-evolving complex of photosystem II, Biochemistry 50 (2011) 6308–6311.

[58] Y. Song, J. Mao, M.R. Gunner, MCCE2: improving protein pK_a calculations with extensive side chain rotamer sampling, J. Comput. Chem. 30 (2009) 2231–2247.

[59] P. Shannon, A. Markiel, O. Ozier, N.S. Baliga, J.T. Wang, D. Ramage, N. Amin, B. Schwikowski, T. Ideker, Cytoscape: a software environment for integrated models of biomolecular interaction networks, Genome Res. 13 (2003) 2498–2504.

[60] J. Lee, X. Cheng, J.M. Swails, M.S. Yeom, P.K. Eastman, J.A. Lemkul, S. Wei, J. Buckner, J.C. Jeong, Y. Qi, S. Jo, V.S. Pande, D.A. Case, C.L. Brooks, A. D. MacKerell, J.B. Klauda, W. Im, CHARMM-GUI input generator for NAMD, GROMACS, AMBER, OpenMM, and CHARMM/OpenMM simulations using the CHARMM36 additive force field, J. Chem. Theory Comput. 12 (2016) 405–413.

[61] F. Guerra, S. Adam, A.-N. Bondar, Revised force-field parameters for chlorophyll-a, pheophytin-a and plastoquinone-9, J. Mol. Graph. Model. 58 (2015) 30–39.

[62] P. Eastman, J. Swails, J.D. Chodera, R.T. McGibbon, Y. Zhao, K.A. Beauchamp, L.-P. Wang, A.C. Simmonett, M.P. Harrigan, C.D. Stern, R.P. Wiewiora, B.R. Brooks, V.S. Pande, OpenMM 7: rapid development of high performance algorithms for molecular dynamics, PLoS Comput. Biol. 13 (2017), e1005659.

[63] N. Michaud-Agrawal, E.J. Denning, T.B. Woolf, O. Beckstein, MDAnalysis: a toolkit for the analysis of molecular dynamics simulations, J. Comput. Chem. 32 (2011) 2319–2327.

[64] J. Lu, M.R. Gunner, Characterizing the proton loading site in cytochrome c oxidase, Proc. Natl. Acad. Sci. U. S. A. 111 (2014) 12414–12419.

[65] Y. Zhang, K. Haider, D. Kaur, V.A. Ngo, X. Cai, J. Mao, U. Khaniya, X. Zhu, S. Noskov, T. Lazaridis, M.R. Gunner, Characterizing the water wire in the gramicidin channel found by Monte Carlo sampling using continuum electrostatics and in molecular dynamics trajectories with conventional or polarizable force fields, J. Theor. Comput. Chem. 2042001 (2020).

[66] S. Braun-Sand, A. Burykin, Z.T. Chu, A. Warshel, Realistic simulations of proton transport along the Gramicidin Channel: demonstrating the importance of solvation effects, J. Phys. Chem. B 109 (2005) 583–592.

[67] I. Ghosh, G. Banerjee, C.J. Kim, K. Reiss, V.S. Batista, R.J. Debus, G.W. Brudvig, D1-S169A substitution of photosystem II perturbs water oxidation, Biochemistry 58 (2019) 1379–1387.

[68] G. Banerjee, I. Ghosh, C.J. Kim, R.J. Debus, G.W. Brudvig, Substitution of the D1-Asn87 site in photosystem II of cyanobacteria mimics the chloride-binding characteristics of spinach photosystem II, J. Biol. Chem. 293 (2018) 2487–2497.

[69] R.J. Debus, Evidence from FTIR difference spectroscopy that D1-Asp61 influences the water reactions of the oxygen-evolving Mn_4CaO_5 cluster of photosystem II, Biochemistry 53 (2014) 2941–2955.

[70] R. Pokhrel, R.J. Service, R.J. Debus, G.W. Brudvig, Mutation of lysine 317 in the D2 subunit of photosystem II alters chloride binding and proton transport, Biochemistry 52 (2013) 4758–4773.

[71] R.J. Service, W. Hillier, R.J. Debus, Evidence from FTIR difference spectroscopy of an extensive network of hydrogen bonds near the oxygen-evolving Mn_4Ca cluster of photosystem II involving D1-Glu65, D2-Glu312, and D1-Glu329, Biochemistry 49 (2010) 6655–6669.

[72] P.L. Dilbeck, H. Bao, C.L. Neveu, R.L. Burnap, Perturbing the water cavity surrounding the manganese cluster by mutating the residue D1-valine 185 has a strong effect on the water oxidation mechanism of photosystem II, Biochemistry 52 (2013) 6824–6833.

[73] R. Nagao, H. Ueoka-Nakanishi, T. Noguchi, D1-Asn-298 in photosystem II is involved in a hydrogen-bond network near the redox-active tyrosine Y_Z for proton exit during water oxidation, J. Biol. Chem. 292 (2017) 20046–20057.

[74] R.J. Debus, FTIR studies of metal ligands, networks of hydrogen bonds, and water molecules near the active site Mn_4CaO_5 cluster in photosystem II, Biochim. Biophys. Acta Bioenerg. 1847 (2015) 19–34.

[75] C.J. Kim, R.J. Debus, Roles of D1-Glu189 and D1-Glu329 in O_2 formation by the water-splitting Mn_4Ca cluster in photosystem II, Biochemistry 59, 40 (2020) 3902–3917.

[76] I. Rivalta, M. Amin, S. Luber, S. Vassiliev, R. Pokhrel, Y. Umena, K. Kawakami, J.-R. Shen, N. Kamiya, D. Bruce, G.W. Brudvig, M.R. Gunner, V.S. Batista, Structural–functional role of chloride in photosystem II, Biochemistry 50 (2011) 6312–6315.

[77] R. Pokhrel, R.J. Debus, G.W. Brudvig, Probing the effect of mutations of asparagine 181 in the D1 subunit of photosystem II, Biochemistry 54 (2015) 1663–1672.

[78] Y. Shimada, H. Suzuki, T. Tsuchiya, M. Mimuro, T. Noguchi, Structural coupling of an arginine side chain with the oxygen-evolving Mn_4Ca cluster in photosystem II as revealed by isotope-edited Fourier transform infrared spectroscopy, J. Am. Chem. Soc. 133 (2011) 3808–3811.

[79] J.P. McEvoy, G.W. Brudvig, Structure-based mechanism of photosynthetic water oxidation, Phys. Chem. Chem. Phys. 6 (2004) 4754–4763.

[80] C.A. Fitch, G. Platzer, M. Okon, B.E. Garcia-Moreno, L.P. McIntosh, Arginine: its pKa value revisited, Protein Sci. 24 (2015) 752–761.

[81] R.J. Service, W. Hillier, R.J. Debus, Network of hydrogen bonds near the oxygen-evolving Mn_4CaO_5 cluster of photosystem II probed with FTIR difference spectroscopy, Biochemistry 53 (2014) 1001–1017.

[82] T. Takaoka, N. Sakashita, K. Saito, H. Ishikita, pK_a of a proton-conducting water chain in photosystem II, J. Phys. Chem. Lett. 7 (2016) 1925–1932.

[83] Y. Shimada, T. Kitajima-Ihara, R. Nagao, T. Noguchi, Role of the O_4 channel in photosynthetic water oxidation as revealed by Fourier transform infrared difference and time-resolved infrared analysis of the D1-S169A mutant, J. Phys. Chem. B 124 (2020) 1470–1480.

[84] H. Suzuki, J. Yu, T. Kobayashi, H. Nakanishi, P.J. Nixon, T. Noguchi, Functional roles of D2-Lys317 and the interacting chloride ion in the water oxidation reaction of photosystem II as revealed by Fourier transform infrared analysis, Biochemistry 52 (2013) 4748–4757.

[85] K. Saito, J.-R. Shen, T. Ishida, H. Ishikita, Short hydrogen bond between redox-active tyrosine $Y_{(Z)}$ and D1-His190 in the photosystem II crystal structure, Biochemistry 50 (2011) 9836–9844.